Aquatic Botany 197 (2025) 103838

Contents lists available at ScienceDirect

Aquatic Botany

journal homepage: www.elsevier.com/locate/aquabot

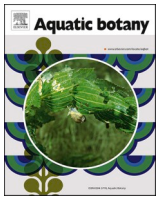

Micro- and ultrastructural features for the distinction of *Phymatolithon lusitanicum* from *Phymatolithon calcareum*

Francesca Panizzuti [a,*], Aurora Giorgi [b], Maggie D. Johnson [b], Daniela Basso [a]

[a] Department of Earth and Environmental Sciences, University of Milan-Bicocca, Milan 20126, Italy
[b] Biological and Environmental Science and Engineering Division, Red Sea Research Center, King Abdullah University of Science and Technology, Thuwal 23955-6900, Saudi Arabia

ARTICLE INFO

Keywords:
Phymatolithon calcareum
Phymatolithon lusitanicum
Integrated taxonomy
Cell fusions
Ultrastructures

ABSTRACT

Calcifying red algae foster unique and rich biological communities and are important component of the global C cycle. Rhodolith beds are globally distributed biodiversity hotspots that are engineered by free-living calcifying red algae, and maërl beds are a type of rhodolith bed typically characterized by free-living, twig-like coralline algae with a branched growth form. *Phymatolithon calcareum,* along with the more recently described *Phymatolithon lusitanicum* is considered a major component of maërl beds in Europe. Here, we explore the morphology of the vegetative thallus of *P. calcareum* and *P. lusitanicum*. Our aim is to identify statistically valuable morphological features that can be used to differentiate these two species of algae that are macroscopically very similar, frequently sterile, and share the same habitat. Morphological features have historically failed to aid in distinguishing *P. lusitanicum* from *P. calcareum*. Our observations of seasonal growth patterns, the arrangement of perithallial cells in filaments, and the size of cell fusions provide noteworthy advances in our ability to use morphological features to identify the different species. Additionally, ultrastructural characteristics appear to be a reliable distinguishing feature between the two *Phymatolithon* species.

1. Introduction

Rhodolith beds are globally distributed biodiversity hot spots that have been described in polar (Teichert et al., 2014), temperate (Chimienti et al., 2020, Rendina et al., 2020) and tropical regions (Moura et al., 2021), ranging from the low intertidal zone to depths of around 150 m and a maximum depth of 290 m (Foster et al., 2013, Rendina et al., 2022). Rhodoliths are unattached nodules formed mostly by non-geniculate coralline algae (Corallinophycidae, Rhodophyta) that create a complex three-dimensional framework (Steller et al., 2003, Foster et al., 2013, Tuya et al., 2023).

Rhodolith beds are ecologically valuable and important in climate regulation, through their roles as hot spots of carbonate production and deep benthic primary production (Basso, 2012, Basso et al., 2016). Rhodoliths act as ecosystem engineers of the bed habitat, and, by providing hard substrates for epiphytic algae and a variety of benthic invertebrates, they foster unique and rich biological communities (Otero-Ferrer et al., 2019, Teichert, 2014, Adams et al., 2020, Rendina et al., 2022, Tuya et al., 2023). The accumulation and eventual stabilization of rhodoliths by crustose coralline algae and bio-constructing marine invertebrates can further the development of these environments into hard substrates and complex habitats. Examples of ecologically significant environments that may form by the stabilization of rhodolith beds are the coralligenous formations in the Mediterranean Sea (Basso, 1998, Basso et al., 2007) and the stable reefs in the Atlantic Ocean (Ávila et al., 2013, Pereira-Filho et al., 2015, Rendina et al., 2022). Among rhodolith beds, maërl beds, such as those in the northeastern Atlantic Ocean (Peña and Bárbara, 2008, 2009, Peña et al., 2014) and the Mediterranean Sea (Gambi et al., 2009, Agnesi et al., 2011, Savini et al., 2012, Basso et al., 2017, Bracchi et al., 2021), are typically characterized by free-living, twig-like branching coralline algae (Sordo et al., 2020).

The genera *Phymatolithon* Foslie and *Lithothamnion* Heydrich have been regarded as significant contributors to the rhodolith beds along the Atlantic European coast. Various species within these genera have been identified as dominant components of these habitats, spanning from Ireland to Spain and extending from the littoral zone down to depths of 55 m (Chamberlain and Irvine 1994, Bressan and Babbini, 2003, Peña

* Corresponding author.
E-mail addresses: francesca.panizzuti@unimib.it (F. Panizzuti), aurora.giorgi@kaust.edu.sa (A. Giorgi), maggie.johnson@kaust.edu.sa (M.D. Johnson), daniela.basso@unimib.it (D. Basso).

https://doi.org/10.1016/j.aquabot.2024.103838
Received 13 June 2024; Received in revised form 21 November 2024; Accepted 22 November 2024
Available online 26 November 2024

et al., 2015). In particular, *Phymatolithon calcareum* (Pallas) W.H.Adey & D.L.McKibbin ex Woelkering & L.M.Irvine 1986 and *Lithothamnion corallioides* (P. Crouan and H. Crouan) P. Crouan and H. Crouan 1867 are considered the major components of maërl beds in Europe, along with *Mesophyllum sphaericum* V. Peña, I. Bárbara, W. H. Adey, Riosmena-Rodrigues and H. G. Choi 2011 and *Phymatolithon lusitanicum* V.Peña 2015 (Peña et al., 2015).

P. lusitanicum was described for the first time as a new maërl species based on an integrative systematic approach that included molecular (COI-5P, *psb*A) and morphological data obtained from recent collections, as well as comparisons to type material from the morphologically and ecologically congruent northeastern Atlantic species *Phymatolithon lamii (*Me. Lemoine) Y.M.Chamberlain 1991 and *Phymatolithon laevigatum* (Foslie) Foslie 1898 (Peña et al., 2015). *P. lusitanicum* has already proven to be a significant component of the maërl beds of the European Atlantic, and even the dominant species in the maërl beds of Atlantic Portugal coasts (Peña et al., 2015, Sordo et al., 2016). Abundances may still be underestimated due to previous difficulties in morphologically discerning. *P. lusitanicum* and *P. calcareum* (Peña and Bárbara, 2008, Hall-Spencer et al., 2010, Peña et al., 2015).

Despite the potential for molecular tools to provide quicker and reliable results for taxonomic identifications, those methods are not always possible. For instance, cases involving poorly preserved or very old material from which DNA cannot be extracted, such as from ancient collections and in the fossil record, may still require species to be identified by morphoanatomical taxonomic features (Basso, 1995, Bracchi et al., 2021). Accordingly, a study by Auer and Piller (2020) highlighted the need for detailed investigations of micro- and nanoscale phenotypic characters (ultrastructures) and their potential to facilitate the integration of morphological and molecular taxonomy. In fact, enhancing morpho-taxonomic concepts, employed in both modern taxonomy and the fossil record, enables the integration of paleontological record with modern molecular phylogeny, facilitating a comprehensive synthesis of historical and present-day species distribution data (Basso, 2012, Auer and Piller, 2020). Therefore, linking morpho- and molecular techniques is crucial for advancing our understanding of coralline algae biodiversity across temporal scales, as well as better investigating the ecological history of coralline algae-dominated ecosystems (Basso, 1995; Auer and Piller, 2020).

Ultimately, such ultrastructural approaches can also provide independent information and verification in cases of conflicting molecular phylogenies (Auer and Piller, 2020).

In the main maërl-forming species of temperate Atlantic European beds (Peña et al., 2015), *P. calcareum*, specimens are predominantly sterile. Sporangial conceptacles (asexual conceptacles) have been seldom reported, and gametangial conceptacles (sexual conceptacles) are even more rare (Woelkerling and Irvine, 1986, Irvine and Chamberlain, 1994, Mendoza and Cabioch, 1998, Peña et al., 2014, Pardo et al., 2017). Similarly, reproductive structures have rarely been found in *P. lusitanicum*, with no observations of sexual uniporate conceptacles (Peña et al., 2015), and vegetative fragmentation of their thalli seems to be the main method of propagation (Peña et al., 2015, Pardo et al., 2017). Although reproductive structures are key features in species delimitation, for instance in distinguishing *P. lusitanicum* from other *Phymatolithon* species (Peña et al., 2015), they can be of limited utility in instances where such reproductive structures are absent.

Here, we explore the morphology of the vegetative thallus of *P. calcareum* and *P. lusitanicum* with the aim of finding statistically valuable morphological features to assist in separating two species of algae that are macroscopically very similar, frequently sterile, and share the same habitat (Peña et al., 2015). By focusing on micro- and ultrastructures, which are inherent characteristics of the vegetative thallus and consistently present, we identify an effective method to separate the two species using only sterile specimens. Additionally, we describe supplementary features that are not historically used for morpho-taxonomy.

2. MATERIALS AND METHODS

2.1. Sampling collection

Maërl specimens were collected while SCUBA diving from a single maërl bed in the Atlantic Iberian Peninsula in Galicia, Vigo (Spain) (N 42° 13,363', W 8° 46,712'). Sampling was conducted at a depth of 7 m on the 5th of October 2022, in the framework of the OLCAPP project (AQUACOSM-Plus).

All specimens were air-dried and preserved in zip-lock bags with silica gel until used for molecular and morphological analyses.

Specimens were observed and photographed both using a stereo and a Scanning Electron Microscope (SEM). A subsample of eight similar specimens (same color, size and branch diameter, and growth form) were selected for genetic identification by molecular analyses. Based on their genetic identification, one specimen of *P. calcareum* (DB 951) and one of *P. lusitanicum* (DB 952) were selected for microscopic and ultrastructural analyses of their vegetative thalli.

2.2. Molecular analyses

Dried coralline algae specimens were used for molecular characterization. First, a subsample of each specimen was selected under a stereo microscope to obtain a chip of the thallus free of epiphytes. Then, each alga was ground to powder using a sterile hammer and chisel and then transferred to a sterile 1.5 ML Eppendorf tube. DNA was extracted with the DNeasy® Plant Mini Kit (Qiagen, Germantown, MD, USA) and purified with the Monarch® PCR & DNA Cleanup Kit (New England Biolabs Inc., Ipswich, MA, USA). The quantity and quality of extracted DNA were evaluated using a Nanodrop ND2000 spectrophotometer (ThermoFisher). PCR reaction targeted the *rbc*L gene which was amplified using the primers F321 (Freshwater and Rueness, 1994) and rbcLrev-NEW (Saunders and Moore, 2013) or, alternatively, the reverse primer R1150 (Freshwater and Rueness, 1994) to obtain amplicons of 1086 or 829 bp, respectively. PCR conditions followed Saunders and Moore (2013). PCR success was evaluated by electrophoresis on 1 % agarose gels. Samples were then cleaned up with the Omega BioTek MicroElute Cycle Pure Kit (Omega Bio-Tek Inc, Norcross, GA, USA) and bidirectionally sequenced using Sanger Technology at the Bioscience Core Lab at King Abdullah University of Science and Technology (KAUST).

2.3. Assembly and phylogenetic analyses

Geneious Prime 2021.1.1 (Biomatters, Auckland, New Zealand) was used to visualize, check and correct chromatograms, and to assemble forward and reverse reads to create consensus sequences that were deposited in GenBank (Supplementary Table 1). The eight newly generated sequences, plus additional DNA sequences belonging to type material or topotypes specimens of coralline algae in the Hapalidiaceae family, were downloaded from GenBank and used to create sequence alignments using the Muscle multiple sequence alignment algorithm (Edgar, 2004). The alignment was then exported from Geneious Prime to IQ-TREE (version 2.1.3; Minh et al., 2020) to compute maximum likelihood (ML) analyses using ultrafast bootstrapping (Hoang et al., 2018), with 1000 bootstrap replicates to assess branch support. The analyses were run with a partition by codon position. The tree was rooted with *Lithophyllum incrustans* (accession number KR708580) and visualized in MEGA 10.1.8 (Kumar et al., 2018; Stecher et al., 2020).

2.4. Morphological analyses

Samples were prepared for SEM observations by breaking the rhodolith branches with a small chisel. Longitudinally cut fragments were chosen for SEM observations, as longitudinal axial sections of branches are a standard representation for coralline algae (Woelkerling, 1988, Quaranta et al., 2007,Burdett et al., 2011, Bracchi et al., 2021). The

selected specimens were mounted on the stubs with graphite paste (Leit-C conductive carbon cement, Neubauer Chemicalen) and then chrome-coated. SEM images were taken with a field emission gun scanning electron microscope (SEM-FEG), Zeiss Gemini 500 at the microscopy platform of the University of Milano-Bicocca.

Anatomical terminology follows Basso (1995), which is in agreement with Cabioch (1972), Adey and Adey (1973), and Johansen (1981). Growth form terminology follows Woelkerling et al. (1993).

The length of each cell was taken as the distance between the two primary pit-connections, and the diameter as the distance between the relevant cell walls (meaning the secondary wall and half of the primary wall separating adjacent cells), perpendicular to the length and at the cell's midline as in Fig. 1a. The thickness of the calcified cell wall was taken as half of the difference between the cell diameter and the cell lumen diameter (Fig. 1b).

Cell fusion measurements were taken as the percentage of the cell length occupied by the fusion length, measured as in Fig. 1b.

Following Bracchi et al. (2021), in this study the term 'ultrastructure' is used to identify the singular crystal in one of the layers of the cell wall, and 'ultrastructural pattern' to indicate the combination and mutual organization of crystals in layers of the cell wall.

Ultrastructures were measured at a standard magnification of 50000X in two dimensions (Fig. 1c), with the rigorous control over cell orientation that is required to represent, describe and measure in two-dimensions the main features of a three-dimensional structure, such as cell calcification (Woelkerling, 1988, Quaranta et al., 2007, Bracchi et al., 2021).

This study is based on a total of 205 SEM pictures that allowed the measurement of 249 cells, 60 cell fusions and 224 crystals. All measurements were made with image analysis software ImageJ.

2.5. Statistical analyses

Pearson's coefficient and the Pearson correlation test were used to assess the statistical relationship between cell measurements (morphometry and cell wall thickness) and ultrastructure measurements (length and width). The Shapiro-Wilk test was employed to test each set of measurements for normality, including the size of cell fusions.

Since data of cell and ultrastructures measurements do not follow a normal distribution, the non-parametric Mann-Whitney test was used to assess the statistical significance in the distributions of the measurements between the groups.

A Students t-test was used to compare the cell fusion size.

All statistical analyses were run in Python 3 with Scipy library 1.10.1.

3. RESULTS

3.1. Molecular analyses

In the maximum likelihood tree (Fig. 2), five sequences (Supplementary Table 1) clustered in the *P. calcareum* clade, which included the neotype from Hernández-Kantún et al., 2015 (voucher BM000712373; accession number KX020487) and the lectotype from Peña et al., (2021) (voucher TRH C1–2892; accession number MW536910). Three newly generated sequences were included in the *P. lusitanicum* clade (Supplementary Table 1). This clade was anchored by the presence of a sequence (MH274807) from Adey et al., (2018), whose *psbA* sequence matched the isotype of *P. lusitanicum* from Peña et al., (2015) (voucher GALW015741; KT874588). Collection information and the newly generated *rbc*L sequence accession numbers for the samples used in the study can be found in the supplementary material.

3.2. Morphological analyses

3.2.1. Phymatolithon calcareum (DB 951)

The selected specimen of *P. calcareum* was dark to light pink in color, with branches terete to flattened toward slightly discolored apices (Fig. 3a).

Once cut, the branches presented a zonate micromorphology, characterized by the alternation of a series of shorter and longer cells, consistent with seasonal changes in growth (Fig. 3a). Perithallial cell filaments were more or less radially arranged, with no clear grid-like organization.

No hypothallus was detected in the analysed branches.

The perithallial cells were spherical to ovoid in shape (Fig. 4c).

Short cell length ranged from 6.40 μm to 14.35 μm, with an average of 10.45 μm ± 1.93 μm. Cell diameter was from 5.90 μm to 14.65 μm, with an average of 9.31 μm ± 2.14 μm. The thickness of the calcified cell wall (primary and secondary) ranged from 0.44 μm to 2.05 μm, with an average of 1.03 μm ± 0.30 μm (Table 1).

Long cell length ranged from 8.57 μm to 17.93 μm, with an average of 11.45 μm ± 1.80 μm. Cell diameter was from 7.11 μm to 10.14 μm, with an average of 8.71 μm ± 0.83 μm. The thickness of the long cell calcified wall (primary and secondary) was from 0.61 μm to 1.50 μm, with an average of 1.03 μm ± 0.20 μm (Table 1).

Multiple fusions were common, encompassing up to 7 cells (Fig. 4e) and often replacing the cell walls almost entirely.

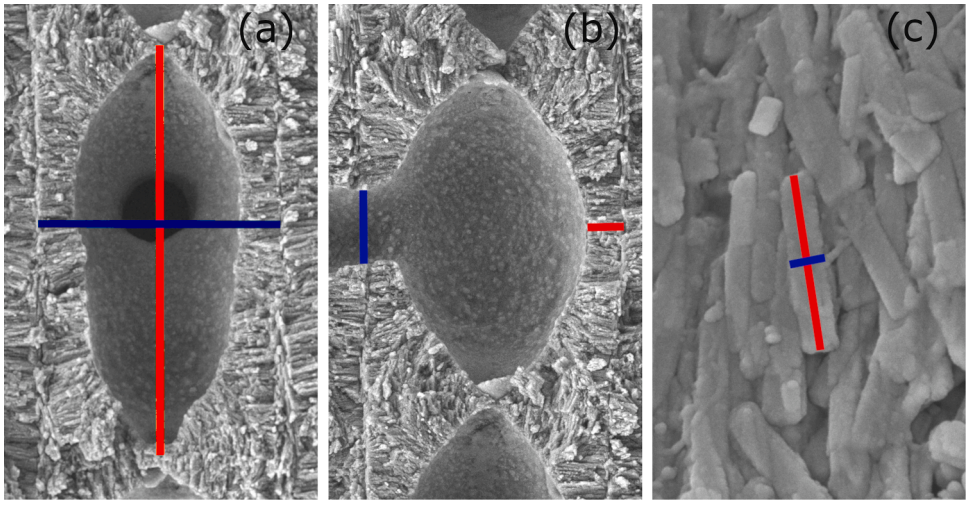

Fig. 1. Micro- and ultrastructures measurements. (a) Cell wall length (red) and diameter (blue). (b) Cell wall thickness (red) and cell fusion (blue). (c) Ultrastructure length (red) and width (blue).

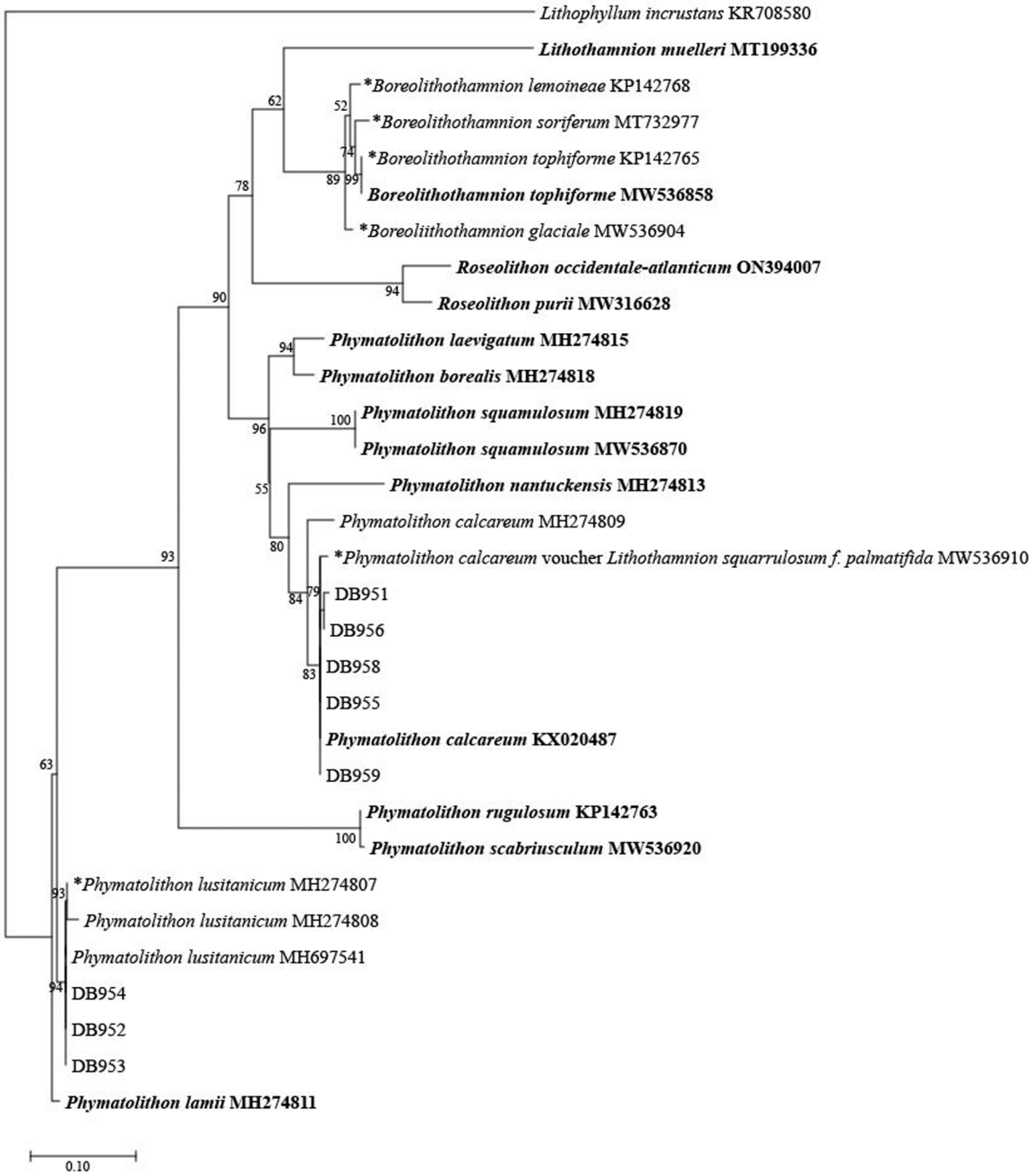

Fig. 2. Maximum likelihood (ML) phylogenetic tree generated from the analyses of the *rbc*L sequences. Numbers at nodes represent bootstrap values from ML analyses. Type specimens are bolded while the presence of a black asterisk before the sequence name indicates a sequence associated with a type. Sequences newly generated in this study are indicated with abbreviation DB and three numbers.

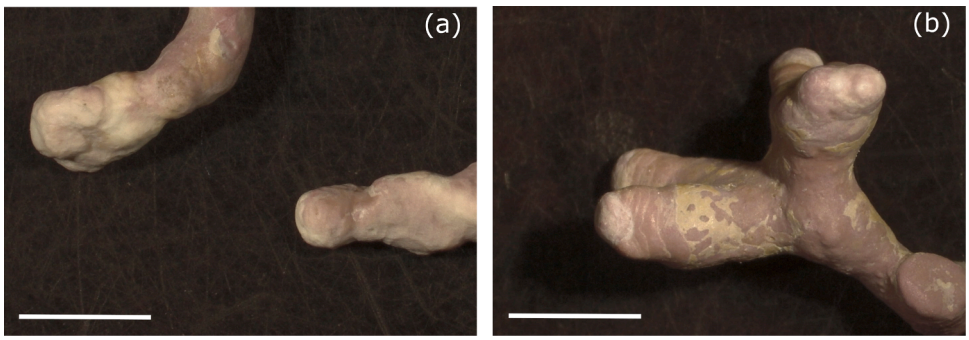

Fig. 3. Branch tips of (a) *P. calcareum* and (b) *P. lusitanicum* under the stereomicroscope. Scale bar = 5 mm.

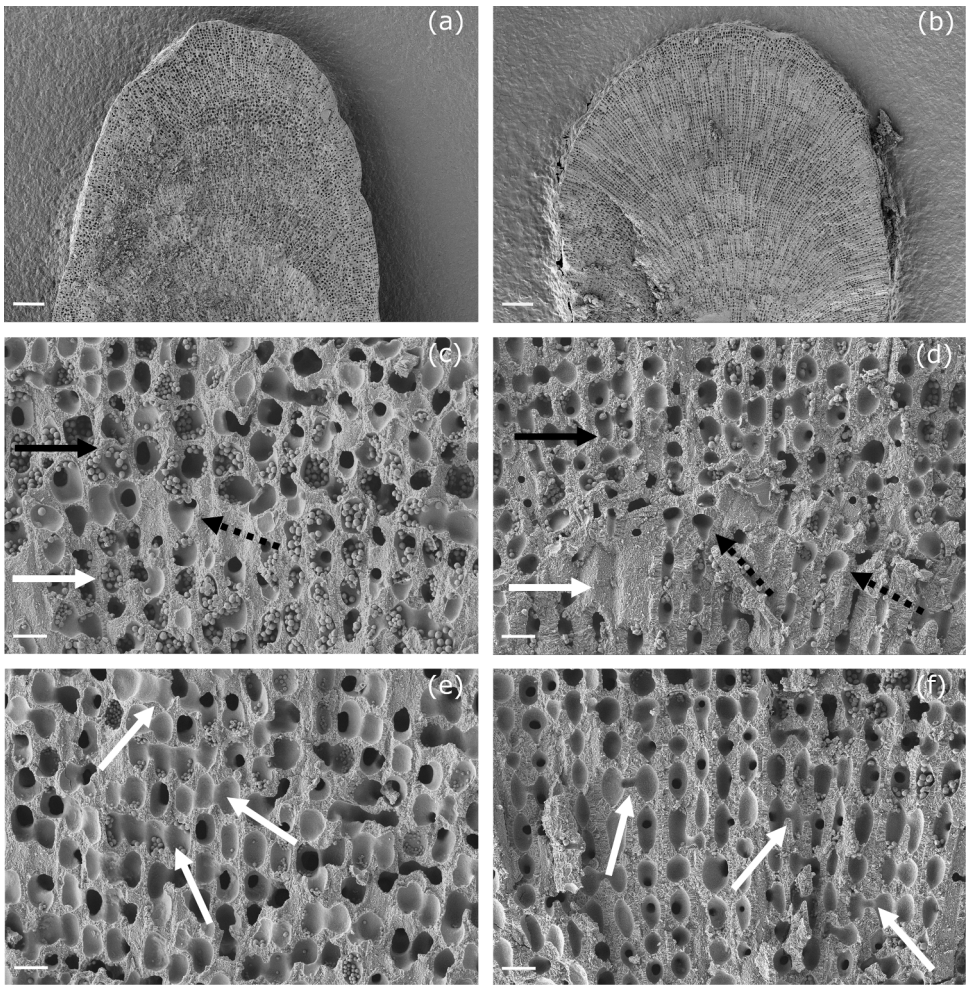

Fig. 4. Comparison of microanatomical features in *P. calcareum* and *P. lusitanicum* under SEM. (a) Longitudinal section of *P. calcareum* with short and long cell zonation. Scale bar = 100 µm. (b) Longitudinal section of *P. lusitanicum* with obvious short and long cell zonation. Scale bar = 100 µm. (c) *P. calcareum*; alternation of short, less calcified, cells (black arrow) and long, more calcified cells (white arrow). Club-shaped cell (dashed arrow). Scale bar = 10 µm. (d) *P. lusitanicum*; alternation of short, less calcified cells (black arrow) and long, more calcified cells (white arrow). Club-shaped cell (dashed arrow). Scale bar = 10 µm. (e) *P. calcareum*; extensive cell fusions (white arrows). Scale bar = 10 µm. (f) *P. lusitanicum*; small cell fusions (white arrows). Scale bar = 10 µm.

Cell fusions occupied from 31 % to 71 % of the length of the cell, with an average of 49 % ±10 % (Table 1).

Club-shaped cells were observed at the transition from the long to the short perithallial cells (Fig. 4c).

Floridean starch was very abundant, mainly concentrated in the central (and older) region of the branch.

The primary wall ultrastructures observed in longitudinal medial sections (cutting the cell lumen) were elongated crystals appearing as rods (Fig. 5a), but where longitudinal sections were tangential to the primary wall, crystals were flat rectangular tiles (Fig. 5c). Globular material (as described in Bracchi et al., 2021) was extensively present between and around the ultrastructures (Fig. 5c). The long axis of the primary wall ultrastructures was parallel to the cell membrane and formed a multi-layered structure. The dimensions of the tiles ranged between 515.05 nm and 1365.43 nm, with an average of 969.52 nm ± 207.69 nm in length, and between 143.12 nm and 314.85 nm, with an average of 220.98 nm ± 35.10 in width (Table 1).

The secondary wall ultrastructures were characterized by elongated crystals oriented radially to the cell lumen in longitudinal cuts (Fig. 5a); these crystals appeared to be formed by small, roundish, units that were fused together (Fig. 5a).

The meristem was characterized by squat-to-roundish cells that were highly variable in dimension (Fig. 6a), with length ranging from 3.83 µm to 8.36 µm and an average of 6.07 µm ± 1.29 µm. The diameter ranged from 5.43 µm to µm 10.32, with an average of 7.62 µm ±1.18 µm. The thickness of the calcified cell wall (primary and secondary wall) ranged from 0.40 µm to µm 1.26, with an average of 0.75 µm ± 0.22 µm (Table 1).

In longitudinal sections, perithallial filaments terminate with 1 (2) epithallial cells. Epithallial cells were flattened to domed (Fig. 6a).

The epithallial cell length ranged from 2.81 µm to 4.87 µm, with an average of 3.96 µm ± 0.65 µm. Cell diameter was from 6.1 µm to 8.72 µm, with an average of 7.83 µm ± 0.87 µm. The thickness of the calcified cell wall (primary and secondary) ranged from 0.47 µm to 1.11 µm, with an average of 0.81 µm ± 0.17 µm (Table 1).

The epithallial cell wall showed similar ultrastructural features to the perithallial cells, with primary wall crystals resembling tiles; abundant roundish globular material was present attached to the crystals, sometimes making it difficult to identify their shape (Fig. 6c).

The dimensions of the tiles ranged between 383.50 nm to 1059.52 nm, with an average of 726.38 nm ± 191.20 nm in length, and between 147.09 nm and 240.78 nm, with an average of 192.52 nm ± 28.22 nm in width (Table 1).

No reproductive structures (conceptacle) were observed.

3.2.2. *Phymatolithon lusitanicum (DB 952)*

The selected specimen of *P. lusitanicum* was pink in color, branching, with rounded, sometimes globular tips showing a folded arrangement of

Table 1
Morphometry of perithallial, meristematic and epithallial cells, wall thickness and cell fusion size measured in longitudinal section, and of primary wall ultrastructures measured in surface tangential sections. Standard deviation in brackets.

			DB 951	DB 952
Perithallus	*Short cells*	Cell Length	10.45 (1.93) µm	9.88 (1.94) µm
		Cell Diameter	9.31 (2.14) µm	8.12 (1.28) µm
		Cell Wall Thickness	1.03 (0.30) µm	1.05 (0.33) µm
	Long cells	Cell Length	11.45 (1.80) µm	11.88 (2.52) µm
		Cell Diameter	8.71 (0.83) µm	8.65 (1.00) µm
		Cell Wall Thickness	1.03 (0.20) µm	1.75 (0.58) µm
	Ultrastructures	Length	969.52 (207.69) nm	749.4 (235.42) nm
		Width	220.98 (35.10) nm	153.36 (41.24) nm
	Cell fusions	Extent	49 % (10 %)	23 % (7 %)
Meristem		Cell Length	6.07 (1.29) µm	5.18 (1.01) µm
		Cell Diameter	7.62 (1.18) µm	7.77 (1.40) µm
		Cell Wall Thickness	0.75 (0.22) µm	0.78 (0.22) µm
Epithallial cells		Cell Length	3.96 (0.65) µm	2.84 (0.69) µm
		Cell Diameter	7.83 (0.87) µm	6.81 (1.30) µm
		Cell Wall Thickness	0.81 (0.17) µm	0.95 (0.31) µm
	Ultrastructures	Length	726.38 (191.20) nm	585.88 (208.83) nm
		Width	192.52 (28.22) nm	168.49 (37.63) nm

layers (Fig. 3b). The surface is smooth matte with flaky white areas that corresponded to the cuticle shedding off (Fig. 3b).

Once cut, the branches were micromorphologically consistent with evident seasonal growth, showing a zonation determined by the alternation of series of shorter cells and longer, more calcified cells (Fig. 4b). Perithallial cell filaments have a mostly regular grid-like and radial organization.

No hypothallus was detected in the analysed branches.

The perithallial long cells were ovoid in shape, with an elongated lumen and heavily calcified walls (Fig. 4d); short cells were ovoid to rectangular in shape, when less calcified (Fig. 4d).

Short cell length ranged from 6.46 µm to 14.84 µm, with an average of 9.88 µm ± 1.94 µm. Cell diameter was from 5.83 µm to 11.23 µm, with an average of 8.12 µm ± 1.28 µm. The thickness of the calcified cell wall (primary and secondary) ranged from 0.47 µm to 1.81 µm with an average of 1.05 µm ± 0.33 µm (Table 1).

Long cell length ranged from 5.65 µm to 17.84 µm, with an average of 11.88 µm ± 2.52 µm. Cell diameter was from 6.10 µm to 10.41 µm, with an average of 8.65 µm ± 1.00 µm. The thickness of the calcified cell wall (primary and secondary) ranged from 0.71 µm to 3.47 µm, with an average of 1.75 µm± 0.58 µm (Table 1).

Multiple fusions were common; they were narrow (consistent with Peña et al., 2015, fig. 14) and encompassing up to 5 cells (Fig. 4f).

Cell fusions occupied from 11 % to 39 % of the length of the cell, with an average of 23 % ±7 % (Table 1).

Club-shaped cells were observed positioned at the transition from the long to the short perithallial cells (Fig. 4d).

Floridean starch was abundant and distributed throughout the whole perithallus.

The primary wall ultrastructures observed in longitudinal medial sections were elongated crystals appearing as rods (Fig. 5b) but where the sections were tangential to the primary wall, crystals were flat, rectangular, defined tiles (Fig. 5d). Globular material was seldom present between and around the ultrastructures (Fig. 5d). The dimensions of the tiles ranged between 215.70 nm and 1213.40 nm, with an average of 749.40 nm ± 235.42 nm in length, and between 41.23 nm and 220.32 nm, with an average of 153.36 nm ± 41.24 nm in width

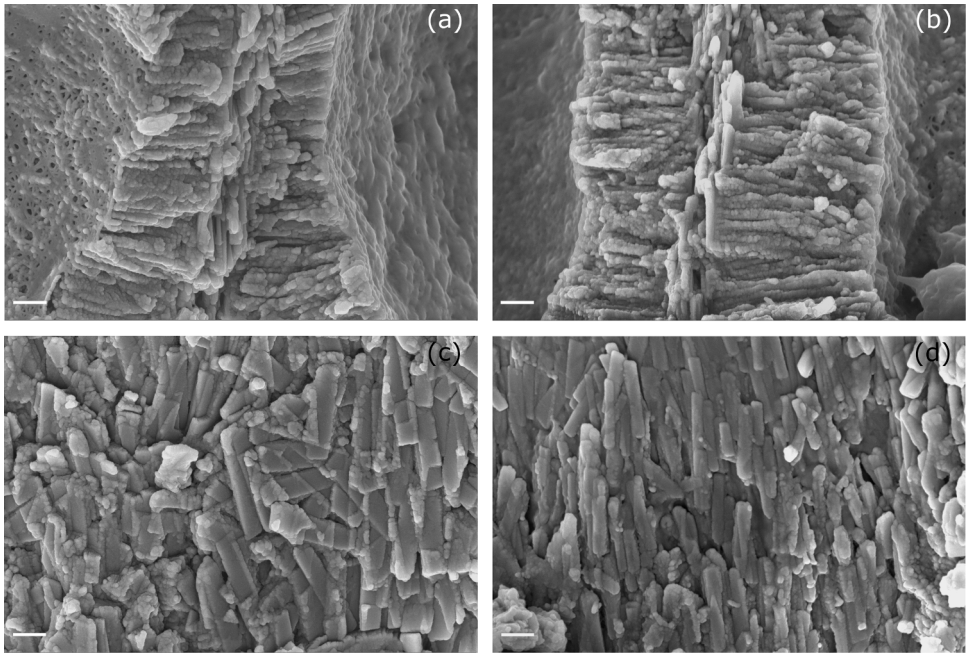

Fig. 5. Comparison of perithallial ultrastructures in *P. calcareum* and *P. lusitanicum* under SEM. (a) *P. calcareum*; Longitudinal section showing the secondary and primary wall ultrastructures. Scale bar = 400 nm. (b) *P. lusitanicum*; Longitudinal section showing the secondary and primary wall ultrastructures. Scale bar = 400 nm. (c) *P. calcareum*; primary wall ultrastructures (rectangular tiles) in tangential section; presence of globular material. Scale bar = 400 nm. (d) *P. lusitanicum*; primary wall ultrastructures (rectangular tiles) in tangential section; scarce presence of globular material. Scale bar = 400 nm.

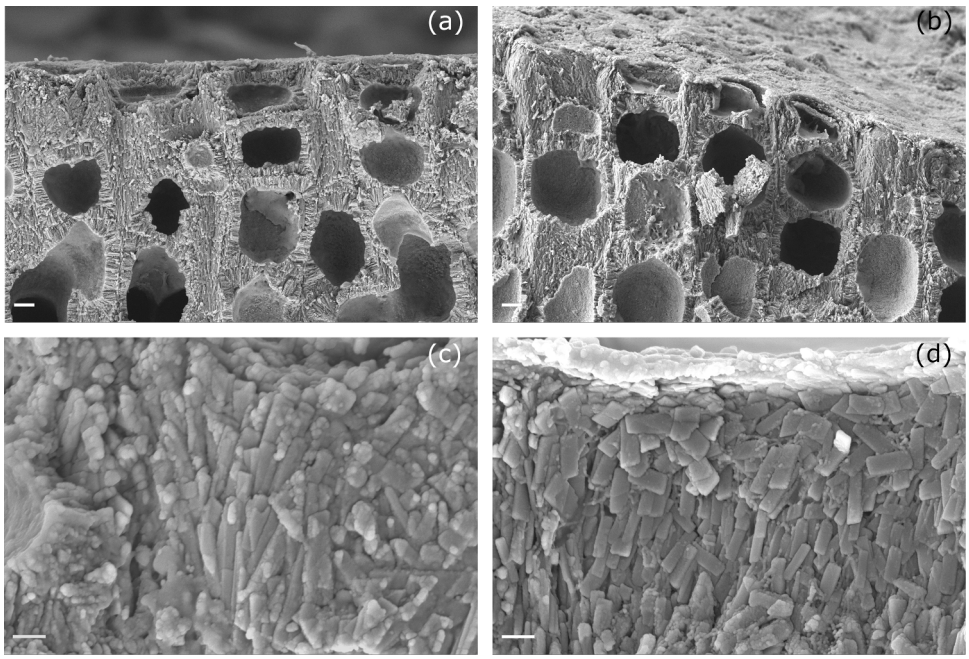

Fig. 6. Comparison of epithallial cells micro- and ultrastructures in *P. calcareum* and *P. lusitanicum* under SEM. (a) *P. calcareum*; epithallial domed cells in longitudinal section. Scale bar = 2 μm. (b) *P. lusitanicum*; epithallial domed cells with narrowing lateral walls in longitudinal section. Scale bar = 2 μm. (c) *P. calcareum*; primary wall ultrastructures (rectangular tiles) in tangential section; presence of abundant globular material. Scale bar = 400 nm. (d) *P. lusitanicum*; primary wall ultrastructures (rectangular tiles) in tangential section; scarce presence of globular material. Scale bar = 400 nm.

(Table 1).

The secondary wall ultrastructures were characterized by elongated crystals oriented radially to the cell lumen in longitudinal cuts (Fig. 5b); these crystals appeared to be formed by small, roundish units that were fused together (Fig. 5b).

The meristem was characterized by squat to rectangular to roundish cells that were highly variable in dimensions, with length ranging from 3.79 μm to 6.70 μm and an average of 5.18 μm ± 1.01 μm. The diameter ranged from 5.33 μm to 9.68 μm, with an average of 7.77 μm ± 1.40 μm. The thickness of the calcified wall (primary and secondary) ranged from 0.45 μm to 1.15 μm, with an average of 0.78 μm ± 0.22 μm (Table 1).

In longitudinal sections, perithallial filaments terminate with 1 (2) epithallial cells. Epithallial cells appeared more or less trapezoidal to ovoidal with a flattened outermost wall and lateral walls narrowing toward the apical part of the cell, consistent with Peña et al. (2015); fig. 14). These lateral walls had no flared out upper edges (sensu Woelkerling, 1988) (Fig. 6b). Epithallial cells often showed collapsed outermost walls.

The cell length ranged from 1.39 μm to 4.28 μm, with an average of 2.84 μm ± 0.69 μm. Cell diameter was from 4.91 μm to 10.06 μm, with an average of 6.81 μm ± 1.30 μm. The thickness of the calcified cell wall (primary and secondary) ranged from 0.44 μm to 1.72 μm, with an average of 0.95 μm ± 0.31 μm (Table 1).

The epithallial cell walls showed similar ultrastructural features to the perithallial cells, with primary wall crystals resembling tiles that varied from a squared to rectangular shape from the apical to the basal part of the epithallial cell (Fig. 6d). Roundish globular material was seldom found attached to the crystals, particularly in the basal part of the epithallial cell.

The dimensions of the tiles ranged between 230.26 nm and 1121.82 nm, with an average of 585.88 nm ± 208.83 nm in length, and between 103.55 nm and 267.01 nm, with an average of 168.49 nm ± 37.63 nm in width (Table 1).

No reproductive structures were observed.

3.2.3. Statistical analyses on morphological parameters

The diameter of the perithallial short cells was significantly larger in *P. calcareum* than in *P. lusitanicum* (Fig. 4c,d), while the differences in cell length and wall thickness were not significant (Tables 2 and 3).

In *P. lusitanicum*, the wall thickness of the perithallial long cells was significantly larger than in *P. calcareum* (Fig. 4c,d), while the differences in cell length and cell wall were not significant (Table 2).

Meristematic cells differences in cell length, cell diameter and wall thickness were not significant (Table 2).

Epithallial cells in *P. calcareum* had significantly larger cell length and cell diameter than *P. lusitanicum* (Fig. 5a,b). The differences in the thickness of the cell calcified wall were not significant (Table 2).

P. calcareum had significantly larger cell fusion size than *P. lusitanicum* (Fig. 4e,f) (Table 2).

In both epithallial and perithallial ultrastructures, length and width were significantly larger in *P. calcareum* than in *P. lusitanicum* (Table 2).

4. DISCUSSION

P. calcareum and *P. lusitanicum* are two of the foundational species of the Atlantic Iberian Peninsula maërl beds (Peña et al., 2015). Before taxonomical analyses were performed (Peña et al., 2015), *P. lusitanicum* was commonly misidentified as *P. calcareum* along the Galician and Portugal coasts (Sordo et al., 2018). This misidentification was due to the impossibility of distinguishing between the two species based on the morphological features historically used to describe coralline algae, with the exception of the external shape of the multiporate asexual (sporangial) conceptacles and its free-living habit as maërl (Peña et al., 2015). In agreement with previous observations about the importance of vegetative reproduction by fragmentation as the primary method of propagation in maërl beds (Pardo et al., 2017, Basso et al., 2016), specimens bearing sporangial or gametangial conceptacles are rarely found (Peña et al., 2015).

In the present study, we employed both classical morphological features and newly described characteristics to discern between *P. lusitanicum* and *P. calcareum*, based solely on the morphology of the vegetative thallus. These morphological differentiations were supported by molecular analyses. An important caveat is that these tools are not intended for distinguishing these species from all other *Phymatolithon*

Table 2
Results of statistical analyses for each morphological feature. Significance at $p < 0.05$ is noted in bold.

	Test	Measurement	Test statistic	p-value	n (DB 951)	n (DB 952)
Perithallus - short cells	Mann-Whitney	Cell length	1001.5	0.0504	37	41
Perithallus - short cells	Mann-Whitney	Cell diameter	1067.5	**0.0095**	37	41
Perithallus - short cells	Mann-Whitney	Cell wall thickness	787.5	0.9232	37	41
Perithallus - long cells	Mann-Whitney	Cell length	843.0	0.1316	31	64
Perithallus - long cells	Mann-Whitney	Cell diameter	1062.0	0.8689	31	64
Perithallus - long cells	Mann-Whitney	Cell wall thickness	169.5	**< 0.0001**	31	64
Perithallus	T-student	Cell fusions extent	0.9714	**< 0.0001**	30	30
Perithallus	Mann-Whitney	Ultrastructure length	3106.0	**<0.0001**	55	74
Perithallus	Mann-Whitney	Ultrastructure width	3701.5	**<0.0001**	55	74
Meristem	Mann-Whitney	Cell length	179.0	0.0937	22	12
Meristem	Mann-Whitney	Cell diameter	116.0	0.5764	22	12
Meristem	Mann-Whitney	Cell wall thickness	121.0	0.7049	22	12
Epithallial cells	Mann-Whitney	Cell length	303.0	**0.0001**	15	23
Epithallial cells	Mann-Whitney	Cell diameter	265.0	**0.0060**	15	23
Epithallial cells	Mann-Whitney	Cell wall thickness	119.0	0.1133	15	23
Epithallial cells	Mann-Whitney	Ultrastructure length	1121.0	**0.0050**	22	73
Epithallial cells	Mann-Whitney	Ultrastructure width	1131.0	**0.0038**	22	73

Table 3
Comparison of *P. calcareum* and *P. lusitanicum* diagnostic features. The vegetative thallus features are from this study. The reproductive anatomy for *P. lusitanicum* is from Peña et al. (2015), while for *P. calcareum* is from Adey and McKibbin, (1970) in Wolf et al. (2016).

				P. calcareum	***P. lusitanicum***
Vegetative thallus	*External morphology and microanatomy*		Growth form	Rhodolith, encrusting, branched	Rhodolith
			Color	Dark to light pink	Pink
			Texture	Smooth matte	Smooth matte with flacky areas
			Tips color	Slightly discolored	Slightly discolored
			Tips shape	Terete to flattened	Rounded sometimes globular with an arrangement of layers
			Filaments organization	Not organized, radial	Grid-like, radial
			Zonation	Yes, not evident	Yes, obvious
	Microstructures	*Perithallial cells*	Long cells	Spherical to ovoid	Ovoid
			Short Cells	Spherical to ovoid	Ovoid to rectangular (when less calcified)
			Cell fusions	Multiple, up to 7	Multiple, up to 5
			Cell fusions extent	49 % (10 %)	23 % (7 %)
			Club shaped cells	Yes	Yes
			Floridean starch	Mainly in the central region of the branch	Throughout the perithallus
		Epithallial cells	Number	1 (2)	1 (2)
			Shape (outermost wall)	Flattened to domed	Flattened to domed
			Shape (in section)	Rectangular to rounded	Trapezoid to ovoidal
	Ultrastructures (primary wall)	*Perithallial cells*	Shape	Rectangular tiles	Rectangular defined tiles
			Orientation	Parallel to the cell wall, parallel and orthogonal to each other	Parallel to each other and to the cell wall
			Globular material	Extensively present	Seldom present
			Length	969.52 (207.69) nm	749.40 (235.42) nm
			Width	220.98 (35.10) nm	153.36 (41.24) nm
		Epithallial cells	Shape	Rectangular tiles	Squared to rectangular defined tiles
			Orientation	Parallel to the cell wall, parallel and orthogonal to each other	Parallel to each other and to the cell wall
			Globular material	Extensively present	Seldom present
			Length	726.38 (191.20) nm	585.88 (208.83) nm
			Width	192.52 (28.22) nm	168.49 (37.63) nm
Reproductive structures	*Sporangial conceptacles*	*Surface view*	Uniporate/ multiporate	Multiporate	Multiporate
			Color	Not described	White
			Rim	Slightly raised	Not conspicuous or raised
			Location	Slightly sunken	Slightly sunken to flush with surface
			Pore plate	Concave to flat	Not described
			Calcified cap	Not described	Yes
			Diameter	Up to 390 µm	130–170 µm
			Number of pores	Up to 60	Up to 30
		Chamber in section	Shape	Elliptical	Elliptical
			Height	58–89 µm	40–70 µm
			Width	126–190 µm	70–166 µm
		Roof in section	Number of cells	4–5	2–3
			Thickness	18–22 µm	12–25 µm
		Buried conceptacles		Not described	Not observed

species, but specifically from each other, given that *P. lusitanicum* and *P. calcareum* are the only two *Phymatolithon* maërl species coexisting in the maërl beds of the Atlantic Iberian Peninsula. Every feature here described should not be used, alone, to differentiate between *P. calcareum* and *P. lusitanicum*, because cannot be individually diagnostic.

In accordance with literature, it was impossible to differentiate *P. lusitanicum* from *P. calcareum* under the stereomicroscope, because both specimens have the same branched growth form and branch size, as well as a pink coloration with paler branch apices and a matte surface.

At low magnifications with SEM, the growth structure and internal zonation of branches can be observed. Both *P. calcareum* and *P. lusitanicum* specimens broadly exhibit a zonate micromorphology determined by alternating shorter and longer cells, which reflects seasonal changes in growth rates (Basso, 1995). It seems logical to infer that the dimensions and calcification of the top layers' cells reflect the season during which the specimens were collected, specifically shortly after the end of summer. Based on this reasoning, what we call short and less calcified cells correspond to the warm season, summer, while the long and more calcified cells correspond to the cold season, winter. This is in contrast with other species, such as *L. corallioides* and *Lithothamnion glaciale* Kjellman 1883, where short cells have more calcified walls with respect to long cells (Bracchi et al., 2021, Kamenos et al., 2017).

Continuing with SEM observations at low magnification, in *P. calcareum* cells are not arranged in clear, orderly filaments, which makes it difficult to observe the zonation. In contrast, *P. lusitanicum* has very regularly-organized cell filaments and the seasonal growth is easily detectable as obvious zonation, providing a first feature that can be possibly useful as a starting point in distinguishing the two species.

At high magnifications at SEM, it is not possible to differentiate *P. calcareum* from *P. lusitanicum* based on the length and diameter of the perithallus cells, also considering short and long cells separately. The only significant difference is the wall thickness of the long cells, where *P. lusitanicum* presents significantly thicker calcified walls than *P. calcareum*. This clearly visible characteristic (Fig. 3d) also shows the transition from long, heavily calcified cells to shorter, less calcified cells in the perithallus of *P. lusitanicum*. In contrast, the long cells in *P. calcareum* have smaller wall thickness to those in *P. lusitanicum* and similar wall thickness compared to the short cells within the same specimen. This reflects the challenges in identifying seasonal zonation at lower magnifications.

Cell fusions were measured in relation to the length of the host cell, to estimate the relative proportion of cell wall occupied by the cell fusion. This is not a feature historically used in morpho-taxonomy, but notably, *P. calcareum* is characterized by obvious and statistically larger cell fusions than *P. lusitanicum*.

The ultrastructures of the primary wall in perithallial cells appear as rectangular tiles, for both specimens, consistent with the description by Auer and Piller (2020) for the genus *Phymatolithon*. The orientation of these tiles, visible in cuts tangential to the cell surface, differ slightly in the two specimens. In *P. lusitanicum*, the ultrastructures were oriented parallel to the cell length and to each other. In contrast, in *P. calcareum* the ultrastructures were oriented parallel to the cell length, but parallel and orthogonal to each other.

Globular material is present among the perithallial ultrastructures in both specimens, with a greater abundance observed in *P. calcareum*. Additionally, *P. calcareum* is characterized by longer and wider ultrastructures than *P. lusitanicum*.

Meristem cells in both *P. calcareum* and *P. lusitanicum* exhibit similar shapes and dimensions, likely attributed to their variable sizes during continuous division (Woelkerling, 1988). Consequently, meristematic cell morphology cannot be a reliable tool to separate the two species.

Epithallial cells belonging to both *P. calcareum* and *P. lusitanicum* have a mainly flattened outermost wall, although they differentiate in longitudinal section. *P. calcareum* epithallial cells are rectangular to rounded and domed in shape, as also described by Adey and McKibbin (1970), while *P. lusitanicum* cells are more or less trapezoidal to ovoidal, with lateral walls narrowing toward the apical part of the cell, but not flared, consistent with Peña et al. (2015). *P. calcareum* cells are significantly longer and larger compared to *P. lusitanicum*, while the calcified wall is thinner.

The ultrastructures of the primary wall in epithallial cells appear as rectangular tiles, as in the perithallus, for both specimens. However, under SEM, their ultrastructure surface differs markedly. *P. lusitanicum* exhibits neat and well-defined ultrastructures, whereas the ultrastructures in *P. calcareum* are covered or fused, with abundant globular material, a characteristic that was also observed in this study in the perithallus ultrastructures of the same specimen.

Finally, in *P. calcareum* the ultrastructural pattern appears disordered, while in *P. lusitanicum* ultrastructures seem to be arranged in three vertical bands that differ for the proportions of the rectangle tile and the presence of some globular material at the basal part of the cell.

P. calcareum exhibits significantly larger and wider ultrastructures, consistent with those of the perithallus, compared to *P. lusitanicum*. The ultrastructural features and the presence of globular material observed in both epithallial and perithallial cells, uniformly distinguishes the two specimens. However, while ultrastructure dimensions can serve as a diagnostic feature, further investigation is needed to understand the exact function of the observed globular material and its potential correlation with crystals formation and size.

Overall, these results emphasize the utility of ultrastructural features as a reliable diagnostic tool for delineating between these two *Phymatolithon* species, although we are aware of the need of further testing on the separation of specimens coming from different maërl beds, because the possibility that different environmental conditions might exert some control on them is untested.

During this study, other observations, such as the localization of floridean starch and the presence of club-shaped cells, were noted but were not subject to quantitative analysis. However, we consider that a systematic survey of these features could open new perspectives and raise new questions.

The distribution of floridean starch, which is visually discernible within the cell lumen under SEM, appears to vary between the two specimens. In *P. calcareum*, the starch is predominantly concentrated in the inner region of the branch, with sporadic presence in other, more superficial regions; conversely, in *P. lusitanicum*, the starch is distributed throughout the perithallus.

Another notable observation pertains to the presence of club-shaped cells precisely positioned at the transition from the long to the short perithallial cells, highlighting the change in lumen shape and calcification pattern of the two cell types. These club-shaped cells exhibit thinner walls in the regions corresponding to the shorter and less calcified cell zone, and thicker walls where they align with the longer and more calcified cell zone, resulting in a distinctive lumen shape reminiscent of a club.

Club-shaped cells are observed in both *P. calcareum* and *P. lusitanicum*, although more obvious in the latter, due to its significant differences in wall thickness between long and short cells.

In conclusion, while historical, classical morphoanatomical features have proven to be of limited utility in distinguishing *P. lusitanicum* from *P. calcareum*, we found that the seasonal growth patterns, the arrangement of perithallial cells in filaments, and the size of cell fusions can yield valuable insight. Further sampling and analyses of specimens from different maërl beds will allow to assess the potential degree of variability of the observed characters caused by the environmental conditions. Our findings are the first, to our knowledge, to characterize cell fusion size as a diagnostic feature for the separation of two coexisting species of the same genus. Cell fusion size may have additional physiological implications, regarding cell wall reabsorption and cell nuclei migration (Cabioch, 1971). Our study presents a novel, integrated approach that combines recently employed features, as ultrastructures, along with entirely new ones, such as cell fusion size. This approach,

complemented by classical morphological characters and molecular analyses, can be used as a model for elucidating crucial characteristics in delineating other ecologically important algal taxa.

CRediT authorship contribution statement

Francesca Panizzuti: Writing – review & editing, Writing – original draft, Visualization, Methodology, Investigation, Formal analysis, Data curation. **Aurora Giorgi:** Writing – review & editing, Writing – original draft, Visualization, Methodology, Investigation, Formal analysis, Data curation. **Maggie D. Johnson:** Writing – review & editing, Writing – original draft, Supervision, Resources, Funding acquisition. **Daniela Basso:** Writing – review & editing, Writing – original draft, Supervision, Resources, Project administration, Methodology, Funding acquisition, Conceptualization.

Declaration of Competing Interest

The authors declare that they have no known competing financial interests or personal relationships that could have appeared to influence the work reported in this paper

Acknowledgements

Francesca Panizzuti is funded by a doctoral fellowship in Environmental Sciences of the Milano-Bicocca University.

We are especially grateful to Paolo Gentile and the microscopy platform of the University of Milano-Bicocca for the expertise and assistance in SEM imaging.

This research made use of the resources of the Core Labs at King Abdullah University of Science & Technology (KAUST). Accordingly, the authors would like to express special gratitude to the Bioscience Core Lab and the Sanger Sequencing Team for their invaluable assistance with the sequencing process.

Daniela Basso was funded by the OACIS project number 4000.1–1 of the Prince Albert II of Monaco Foundation.

We are grateful to Jose Gonzalez Fernandez, University of Vigo for the collaboration in the framework of the OLCAPP project (AQUACOSM-Plus).

Support for sequencing was provided by KAUST baseline funding to Maggie D. Johnson.

Appendix A. Supporting information

Supplementary data associated with this article can be found in the online version at doi:10.1016/j.aquabot.2024.103838.

Data Availability

Data will be made available on request.

References

Adams, L.A., Maneveldt, G.W., Green, A., Karenyi, N., Parker, D., Samaai, T., Kerwath, S., 2020. Rhodolith bed discovered off the south African coast. Diversity 12, 125. https://doi.org/10.3390/d12040125.

Adey, W.H., Adey, P.J., 1973. Studies on the biosystematics and ecology of the epilithic crustose Corallinaceae of the British Isles. Br. Phycol. J. 8, 343–407. https://doi.org/10.1080/00071617300650381.

Adey, W.H., Hernandez-Kantun, J.J., Gabrielson, P.W., Nash, M.C., Hayek, L.C., 2018. Phymatolithon (Melobesioideae, Hapalidiales) in the Boreal–Subarctic Transition Zone of the North Atlantic: A Correlation of Plastid DNA Markers with Morpho-Anatomy, Ecology, and Biogeography. The Smithsonian Institution, Washington, DC.

Adey, W.H., McKibbin, D.L., 1970. Studies on the maërl species *Phymatolithon calcareum* (Pallas) nov: comb. and *Lithothamnion coralloides* Crouan in the Ria de Vigo. Bot. Mar. 13, 100–106. https://doi.org/10.1515/botm.1970.13.2.100.

Agnesi, S., Babbini, L., Bressan, G., Cassese, M.L., Mo, G., Tunesi, L., 2011. Distribuzione della Facies del Maerl e delle associ- azioni a rodoliti nei mari italiani: attuale stato delle conoscenze. Biol. Mar. Medit. 18, 50–51.

Auer, G., Piller, W.E., 2020. Nanocrystals as phenotypic expression of genotypes – an example in coralline red algae. Sci. Adv. 6, eaay2126. https://doi.org/10.1126/sciadv.aay2126.

Ávila, E., Riosmena-Rodríguez, R., Hinojosa-Arango, G., 2013. Sponge–rhodolith interactions in a subtropical estuarine system. Helgol. Mar. Res. 67, 349–357.

Basso, D., 1995. Living calcareous algae by a paleontological approach: the genus *Lithothamnion* Heydrich nom. cons. from the soft bottoms of the Tyrrhenian Sea (Mediterranean). Riv. Ital. di Paleontol. e Stratigr. 101, 349–366.

Basso, D., 1998. Deep rhodolith distributionin the Pontian Islands, Italy: a model for the paleontology of a temperate sea. Paleogeogr. Paleoclimatol. Paleoecol. 137, 173–187. https://doi.org/10.1016/S0031-0182(97)00099-0.

Basso, D., 2012. Carbonate production by calcareous red algae and global change. Geodiversitas 34, 13–33. https://doi.org/10.5252/g2012n1a2.

Basso, D., Babbini, L., Kaleb, S., Bracchi, V., Falace, A., 2016. Monitoring deep Mediterranean rhodolith beds. Aquat. Conserv.: Mar. Freshw. Ecosyst. 26, 549–561. https://doi.org/10.1002/aqc.2586.

Basso, D., Babbini, L., Ramos-Esplá, A.A., Salomidi, M., 2017. Mediterranean Rhodolith Beds. In: Rhodolith/maërl beds: A global perspective. In: Coas. Res. Lib., 15. Springer, Cham, pp. 281–298.

Basso, D., Nalin, R., Massari, F., 2007. Genesis and composition of the Pleistocene Coralligène de plateau of the Cutro Terrace (Calabria, southern Italy). N. Jb. Geol. PaläOnt. 244 (2), 73–182. https://doi.org/10.1127/0077-7749/2007/0244-0173.

Bracchi, V.A., Piazza, G., Basso, D., 2021. A stable ultrastructural pattern despite variable cell size in *Lithothamnion corallioides*. Biogeosciences 18, 6061–6076. https://doi.org/10.5194/bg-18-6061-2021.

Bressan, G., Babbini, L., 2003. Corallinales del mar Mediterraneo: guida alla determinazione. Soc. á Ital. di Biol. Mar. 10, 1–237.

Burdett, H., Kanemos, N.A., Law, A., 2011. Using coralline algae to understand historic marine cloud cover. Paleogeogr. Paleocl. 302, 65–70. https://doi.org/10.1016/j.paleo.2010.07.027.

Cabioch, J., 1971. Étude sur les Corallinacées. I. Caractères généraux de la cytologie. Cab. Biol. Mar. 12, 121–186.

Cabioch, J., 1972. Étude sur les Corallinacées. II. La Morphog. èse; Cons. équences Syst. ématiques Et. phylogéN.étiques. Cah. Biol. Mar. 13, 137–288.

Chimienti, G., Rizzo, L., Kaleb, S., Falace, A., Fraschetti, S., De Giosa, F., Tursi, A., Barbone, E., Ungaro, N., Mastrototaro, F., 2020. Rhodolith beds heterogeneity along the apulian continental shelf (Mediterranean Sea). J. Mar. Sci. Eng. 8, 813. https://doi.org/10.3390/jmse8100813.

Edgar, R.C., 2004. MUSCLE: multiple sequence alignment with high accuracy and high throughput. Nucleic Acids Res 32 (5), 1792–1797. https://doi.org/10.1093/nar/gkh340.

Foster, M.S., Amado-Filho, G.M., Kamenos, K.A., Riosmena-Rodríguez, R., Steller, D.L., 2013. Rhodoliths and rhodolith beds. : Res. Discov.: Res. Discov.: Revolut. Sci. SCUBA 143–155.

Freshwater, D.W., Rueness, J., 1994. Phylogenetic relationships of some European Gelidium (Gelidiales, Rhodophyta) species, based on *rbcL* nucleotide sequence analysis. Phycologia 33, 187–194. https://doi.org/10.2216/i0031-8884-33-3-187.1.

Gambi, M.C., Buia, M.C., Massa-Gallucci, A., Cigliano, M., Lattanzi, L., Patti, F.P., 2009. The "pink mile": benthic assemblages of rhodolith and maërl beds (Corallinales) off the Island of Ischia (Tyrrhenian Sea). In: Pergent-Martini, C., Brichet, M. (Eds.), UNEP-MAP-RAC/SPA, Proceedings of the 1st Mediterranean Symposium on the Conservation of the Coralligenous and Other Calcareous Bio-concretions (Tabarka, 15-16/1/2009), pp. 198–201.

Hall-Spencer, J.M., Kelly, J., Maggs C.A., 2010. Background document for maërl beds. (O.C.B.S. 491/2010, ed.) OSPAR Commission pp. 36.

Hoang, D.T., Chernomor, O., von Haeseler, A., Minh, B.Q., Vinh, L.S., 2018. UFBoot2: Improving the ultrafast bootstrap Approximation. Mol. Biol. Evol. 35, 518–522. https://doi.org/10.1093/molbev/msx281.

Irvine, L.M., Chamberlain, Y.M., 1994. Seaweeds of the British Isles vol. 1: Rhodophyta, Part 2B Corallinales, Hildenbrandiales. The Natural History Museum, London.

Johansen, H.W., 1981. Coralline algae, a first synthesis. CRC Press, Boca Raton, Florida, pp. 239.

Kamenos, N.A., Burdett, H.L., Darrenougue, N., 2017. Coralline Algae as Recorders of Past Climatic and Environmental Conditions. In: Riosmena-Rodríguez, R., Nelson, W., Aguirre, J. (Eds.), Rhodoliths/Maërl beds: A Global Perspective. Springer, Cham, pp. 27–53. https://doi.org/10.1007/978-3-319-29315-8.

Kumar, S., Stecher, G., Li, M., Knyaz, C., Tamura, K., 2018. MEGA X: molecular evolutionary genetics analysis across computing platforms. Mol. Biol. Evol. 35, 1547–1549. https://doi.org/10.1093/molbev/msy096.

Mendoza, M.L., Cabioch, J., 1998. Étude comparée de la reproduction de *Phymatolithon calcareum* (Pallas) Adey & McKibbin et *Lithothamnion corallioides* (P. & H. Crouan) P. & H. Crouan (Corallinales, Rhodophyta), et reconsidérations sur la définition des genres. Can. J. Bot. 76, 1433–1445. https://doi.org/10.1139/b98-116.

Minh, B.Q., Schmidt, H.A., Chernomor, O., Schrempf, D., Woodhams, M.D., von Haeseler, A., Lanfear, R., 2020. IQ-TREE 2: New models and efficient methods for phylogenetic inference in the genomic era. Mol. Biol. Evol. 37, 1530–1534 https://doi. org/10.1093/molbev/msaa015.

Moura, R.L., Abieri, M.L., Castro, G.M., Carlos-Júnior, L.A., Chiroque-Solano, P.M., Fernandes, N.C., Bastos, A.C., 2021. Tropical rhodolith beds are a major and belittled reef fish habitat. Sci. Rep. 11, 1–10.

Otero-Ferrer, F., Mannarà, E., Cosme, M., Falace, A., Montiel-Nelson, J.A., Espino, F., Haroun, R., Tuya, F., 2019. Early-faunal colonization patterns of discrete habitat units: a case study with rhodolith-associated vagile macrofauna. Estuar. Coast. Shelf Sci. 218, 9–22. https://doi.org/10.1016/j.ecss.2018.11.020.

Pardo, C., Bárbara, I., Barreiro, R., Peña, V., 2017. Insights into species diversity of associated crustose coralline algae (Corallinophycidae, Rhodophyta) with Atlantic

European maërl beds using DNA barcoding. An. Jard. Bot. Madr. 72, e059. https://doi.org/10.3989/ajbm.2459.

Peña, V., Bárbara, I., Grall, J., Maggs, C.A., Hall-Spencer, J.M., 2014. The diversity of seaweeds on maërl in the NE Atlantic. Mar. Biodiv. 44 (7), 533–551. https://doi.org/10.1007/s12526-014-0214-.

Peña, V., Bárbara, I., 2008. Maërl community in the north-western Iberian Peninsula: a review of floristic studies and long-term changes. Aq. Cons. Mar. Freshw. Ecos. 18, 339–366. https://doi.org/10.1002/aqc.847.

Peña, V., Bárbara, I., 2009. Distribution of the Galician maërl beds and their shape classes (Atlantic Iberian Peninsula): proposal of areas in future conservation actions. Cah. Biol. Mar. 50, 353–368.

Peña, V., Bélanger, D., Gagnon, P., Richards, J.L., Le Gall, L., Hughey, J.R., Saunders, G. W., Lindstrom, S.C., Rinde, E., Husa, V., Christie, H., Fredriksen, S., Hall-Spencer, J. M., Steneck, R.S., Schoenrock, K.M., Gitmark, J., Grefsrud, E., Anglès d'Auriac, M.B., Legrand, E., Grall, J., Mumford, F., Kamenos, N.A., Gabrielson, P.W., 2021. *Lithothamnion* (Hapalidiales, Rhodophyta) in the changing Arctic and Subarctic: DNA sequencing of type and recent specimens provides a systematics foundation*. Eur. J. Phycol. 56 (4), 468–493. https://doi.org/10.1080/09670262.2021.1880643.

Peña, V., Pardo, C., López, L., Carro, B., Hernandez-Kantun, J., Adey, W.H., Bárbara, I., Barreiro, R., Le Gall, L., 2015. *Phymatolithon lusitanicum* sp. nov. (Hapalidiales, Rhodophyta): The third most abundant maerl-forming species in the Atlantic Iberian Peninsula. Cryptogam. Algol. 36 (4), 429–459. https://doi.org/10.7872/crya/v36.iss4.2015.429.

Pereira-Filho, G.H., Francini-Filho, R.B., Pierozzi Jr, I., Pinheiro, H.T., Bastos, A.C., Moura, R.L., Moraes, F.C., Matheus, Z., da Gama Bahia, R., Amado-Filho, G.M., 2015. Sponges and fish facilitate succession from rhodolith beds to reefs. Bull. Mar. Sci. 91, 45–46.

Quaranta, F., Vannucci, G., Basso, D., 2007. Neogoniolithon contii comb. nov. based on the taxonomic reassessment of Mastrorilli's original collections from the Oligocene of NW Italy (Tertiary Piedmont Basin). Riv. It. Paleont. Strat. 113, 43–55 https://doi.org10.13130/2039-4942/6357.

Rendina, F., Buonocore, E., Cocozza di Montanara, E., Russo, G.F., 2022. The scientific research on rhodolith beds: a review through bibliometric network analysis. Ecol. Inform. 70, 101738. https://doi.org/10.1016/j.ecoinf.2022.101738.

Rendina, F., Kaleb, S., Caragnano, A., Ferrigno, F., Appolloni, L., Donnarumma, L., Russo, G.F., Sandulli, R., Roviello, V., Falace, A., 2020. Distribution and characterization of deep rhodolith beds off the Campania coast (SW Italy, Mediterranean Sea). Plants 9, 985. https://doi.org/10.3390/plants9080985.

Saunders, G.W., Moore, T.E., 2013. [Review] Refinements for the amplification and sequencing of red algal DNA barcode and RedToL phylogenetic markers: a summary of current primers, profiles and strategies. Algae 28 (1), 31–43. https://doi.org/10.4490/algae.2013.28.1.031.

Savini, A., Basso, D., Bracchi, V.A., Corselli, C., Pennetta, M., 2012. Maërl-bed mapping and carbonate quantification on submerged terraces offshores the Cilento peninsula (Tyrrhenian Sea, Italy). Geodiversitas 34, 77–98. https://doi.org/10.5252/g2012n1a5.

Sordo, L., Santos, R., Barrote, I., Silva, J., 2018. High CO_2 decreases the long-term resilience of the free-living coralline algae *Phymatolithon lusitanicum*. Ecol. Evol. 8 (10), 4781–4792. https://doi.org/10.1002/ece3.4020.

Sordo, L., Santos, R., Barrote, I., Freitas, C., Silva, J., 2020. Seasonal photosynthesis, respiration, and calcification of a temperate maërl bed in southern Portugal. Front. Mar. Sci. 7, 136. https://doi.org/10.3389/fmars.2020.00136.

Sordo, L., Santos, R., Reis, J., Shulika, A., Silva, J., 2016. A direct CO_2 control system for ocean acidification experiments: testing effects on the coralline red algae *Phymatolithon lusitanicum*. PeerJ 4, e2503. https://doi.org/10.7717/peerj.2503.

Stecher, G., Tamura, K., Kumar, S., 2020. Molecular evolutionary genetics analysis (MEGA) for macOS. Mol. Biol. Evol. 37, 1237–1239. https://doi.org/10.1093/molbev/msz312.

Steller, D.L., Riosmena-Rodríguez, R., Foster, M.S., Roberts, C.A., 2003. Rhodolith bed diversity in the Gulf of California: the importance of rhodolith structure and consequences of disturbance. Aquat. Conser. Mar. Freshw. Ecosyst. 13, S5–S20. https://doi.org/10.1002/acq.564.

Teichert, S., Woelkerling, W., Rüggeberg, A., Wisshak, M., Piepenburg, D., Meyerhöfer, M., Form, A., Freiwald, A., 2014. Arctic rhodolith beds and their environmental controls (Spitsbergen, Norway). Facies 60, 15–37.

Tuya, F., Schubert, N., Aguirre, J., Basso, D., Bastos, E.O., Berchez, F., Bernardino, A.F., Bosch, N.E., Burdett, H.L., Espino, F., Fernández-Gárcia, C., Francini-Filho, R.B., Gagnon, P., Hall-Spencer, J.M., Haroun, R., Hofmann, L.C., Horta, P.A., Kamenos, N. A., Le Gall, L., Tâmega, F.T.S., 2023. Levelling-up rhodolith-bed science to address global-scale conservation challenges. Sci. Total Environ. 892, 164818 https://doi.org/10.1016/j.scitotenv.2023.164818.

Woelkerling, W.J., 1988. The coralline red algae: an analysis of the genera and subfamilies of non-geniculate Corallinaceae. British Museum (Natural History) and Oxford University Press, London, UK, pp. 268.

Woelkerling, W.J., Irvine, L.M., Harvey, A.S., 1993. Growth-forms in non-geniculate coralline red algae (Corallinales, Rhodophyta). Aust. Syst. Bot. 6, 277–293.

Woelkerling, J.W., Irvine, L.M., 1986. The typification and status of Phymatolithon (Corallinaceae, Rhodophyta). Br. Phycol. J. 21, 55–88. https://doi.org/10.1080/00071618600650071.

Wolf, M.A., Falace, A., Kaleb, S., Moro, I., 2016. Molecular data confirm the existence of attached crustose tetrasporangial thalli in *Phymatolithon calcareum* (Melobesioideae, Hapalidiaceae, Rhodophyta) from the Mediterranean Sea. Aquat. Bot. 134, 75–81. https://doi.org/10.1016/j.aquabot.2016.07.006.